arXiv:1005.3961v1 [cond-mat.soft] 21 May 2010

Phase Diagrams of Binary Mixtures of Oppositely Charged Colloids

Markus Bier*
Max-Planck-Institut für Metallforschung, Heisenbergstraße 3, 70569 Stuttgart, Germany, and Institut für Theoretische und Angewandte Physik, Universität Stuttgart, Pfaffenwaldring 57, 70569 Stuttgart, Germany

René van Roij
Institute for Theoretical Physics, Utrecht University, Leuvenlaan 4, 3584 CE Utrecht, The Netherlands

Marjolein Dijkstra†
Soft Condensed Matter, Debye Institute for NanoMaterials Science Utrecht University, Princetonplein 5, 3584 CC Utrecht, The Netherlands

(Dated: 21 May, 2010)

Phase diagrams of binary mixtures of oppositely charged colloids are calculated theoretically. The proposed mean-field-like formalism interpolates between the limits of a hard-sphere system at high temperatures and the colloidal crystals which minimize Madelung-like energy sums at low temperatures. Comparison with computer simulations of an equimolar mixture of oppositely charged, equally sized spheres indicate semi-quantitative accuracy of the proposed formalism. We calculate global phase diagrams of binary mixtures of equally sized spheres with opposite charges and equal charge magnitude in terms of temperature, pressure, and composition. The influence of the screening of the Coulomb interaction upon the topology of the phase diagram is discussed. Insight into the topology of the global phase diagram as a function of the system parameters leads to predictions on the preparation conditions for specific binary colloidal crystals.

PACS numbers: 64.70.pv, 64.70.D-, 64.70.K-

I. INTRODUCTION

Colloidal suspensions are interesting experimental realizations of many-particle systems because, in contrast to molecules, they are directly accessible to observations and the interactions can be tuned in a wide range by means of the preparation procedure and the experimental conditions [1–4]. The flexibility of colloidal suspensions, however, implies many system parameters to be specified, such as size and shape of the colloids as well as strength and functional form of the interaction potential [5–8]. In addition, the number of parameters increases enormously if one considers mixtures of different colloidal species instead of a pure system of only one type of colloid. Moreover, the dimension of the phase diagram increases in parallel with the number of colloidal species in the suspension. The high dimensionality of the parameter space and the phase diagrams call for a simple theory to get an overview of the global phase behavior of colloidal suspensions because a systematic scan by means of experiments or computer simulations is precluded.

In the present work such a simple theory is formulated for the case of binary mixtures of spherical colloids of the same radius and opposite charges of equal magnitude. The global phase diagrams for this setting are in terms of the temperature, the pressure, and the composition and there is only one additional parameter describing the screening of the Coulomb interaction. The reason to consider this comparatively low-dimensional problem here is that the reliability of the approach should be assessed with respect to available results on special cases obtained by means of computer simulations [9, 10] and Madelung sum calculations [7, 11, 12]. An extension of the method to multi-component, size- and charge-polydisperse colloidal suspensions is readily achieved along the same lines.

The proposed mean-field-like formalism correctly interpolates between the hard-sphere limit at high temperatures and a Madelung-type description at low temperatures. As a mean-field theory, the present approach underestimates fluctuations such that critical phenomena and quantitative aspects of phase transitions are covered in lowest order only. The over-all topology of the phase diagram, in particular the types of phases present, however, is not expected to be influenced qualitatively. The simple and transparent formalism turns out to be in semi-quantitative agreement with the computer simulation results of Ref. [10]; this gives confidence that a possible extension to multi-component, size- and charge-polydisperse colloidal suspensions leads to a reliable description.

The model, the formalism, and further technical details are introduced in Sec. II. Results are discussed in Sec. III and Sec. IV concludes with a summary.

---

*Electronic address: bier@mf.mpg.de
†Electronic address: m.dijkstra1@uu.nl

II. FORMALISM

A. Model

Consider a binary mixture of N_1 positively charged colloids and N_2 negatively charged colloids in a solvent of volume V, temperature T, Debye screening length κ^{-1}, and dielectric constant ε. For simplicity we restrict attention to equally sized spherical colloids of radius a with exactly opposite valency $Z_1 = Z > 0$ and $Z_2 = -Z < 0$ for the positively and negatively charged colloids, respectively. For later use we define the sign of the colloidal charge $q_i = Z_i/Z, i \in \{1, 2\}$. The thermodynamic state can be characterized by the total volume fraction $\phi = 4\pi a^3 N/(3V)$ and the mole fraction of the positively charged colloids $x_1 = x = N_1/N$ where $N = N_1 + N_2$ is the total number of colloids; the mole fraction of the negatively charged colloids is given by $x_2 = 1 - x$. The osmotic pressure p will be reported in terms of the dimensionless combination $p^* = 4\pi p a^3/(3k_B T)$ where k_B is the Boltzmann constant. The effective colloidal interactions are assumed to be pairwise additive with hard-core and screened-Coulomb contributions but without Van der Waals attractions; these conditions are realized in index-matched solvents. In terms of the dimensionless temperature $T^* = 4\pi\varepsilon_0\varepsilon k_B T a(1 + \kappa a)^2/(Ze)^2$ with the permittivity of the vacuum ε_0 and the elementary charge e, the pair potential can thus be written as

$$\beta U_{ij}(r) = \begin{cases} \infty & , r < 2a \\ \dfrac{q_i q_j}{T^*} \dfrac{\exp(-\kappa a(r/a - 2))}{r/a} & , r \geq 2a \end{cases}, \quad (1)$$

where $\beta = 1/(k_B T)$ is the inverse temperature.

B. Gibbs free energy

The phase behavior of the system under consideration will be calculated from the Gibbs free energy per particle per $k_B T$

$$g(T^*, p^*, x) = f(T^*, \Phi(T^*, p^*, x), x) + \frac{p^*}{\Phi(T^*, p^*, x)}, \quad (2)$$

where $f(T^*, \phi, x)$ is the Helmholtz free energy per particle per $k_B T$ and $\Phi(T^*, p^*, x)$ is the total volume fraction for given (T^*, p^*, x), which is implicitly defined by means of the equation of state

$$p^* = \phi^2 \frac{\partial f}{\partial \phi}\bigg|_{\phi=\Phi(T^*,p^*,x)}. \quad (3)$$

Below $f(T^*, \phi, x)$, and hence $g(T^*, p^*, x)$ using Eqs. (2) and (3), is calculated for (i) fluid, (ii) crystalline, and (iii) substitutionally disordered solid phases. The expressions involve a priori unknown constants which are fixed by fitting to the well-known hard-sphere fluid-crystal transition.

1. Fluid phase

The Helmholtz free energy per particle of the fluid phase is approximated by the analytical solution of the mean spherical approximation (MSA) of hard-sphere Yukawa mixtures [13]

$$\begin{aligned} f(T^*, \phi, x) &= c_f + \sum_i x_i \ln(x_i) + \ln(\phi) + \frac{\phi(4 - 3\phi)}{(1 - \phi)^2} \\ &\quad + \frac{B(\Gamma)}{2T^*} + \frac{\Gamma^2(\Gamma + 3\kappa a)}{18\phi} \end{aligned} \quad (4)$$

with the integration constant c_f, which will be fixed below, the excess internal energy due to the screened-Coulomb interaction $B(\Gamma)$ given by Eq. (14) of Ref. [13], and the effective screening strength Γ being the non-negative solution of the 6th-order algebraic equation (10) of Ref. [13], which has to be solved numerically. Upon $T^* \to \infty$ one finds $\Gamma \to 0$ such that Eq. (4) leads to the Carnahan-Starling equation of state [14].

2. Crystalline phases

The Helmholtz free energy per particle of crystalline phases is approximated by the following mean-field functional of the one-particle density profiles $\varrho_i, i \in \{1, 2\}$, where $\varrho_i(\mathbf{r})$ is the number density of positively ($i = 1$) or negatively ($i = 2$) charged colloids at position $\mathbf{r}$ in space:

$$\begin{aligned} &f(T^*, \phi) - f^{\text{hs}}(\phi) \\ &= \frac{1}{2N} \int\limits_V \mathrm{d}^3 r \int\limits_{V(\mathbf{r})} \mathrm{d}^3 r' \sum_{i,j} \varrho_i(\mathbf{r})\varrho_j(\mathbf{r}')\beta U_{ij}(|\mathbf{r}' - \mathbf{r}|). \end{aligned} \quad (5)$$

Here f^{hs} is the hard-sphere Helmholtz free energy per particle per $k_B T$ in the crystalline phase, V is the system volume, and $V(\mathbf{r}) = \{\mathbf{r}' \in V : |\mathbf{r}' - \mathbf{r}| \geq 2a\}$. Note that the concentration x of a crystal is fixed by the crystal structure and not a free parameter. Given the crystal structure $\mathcal{C} = \mathcal{C}_1 \cup \mathcal{C}_2$ composed of the sublattices $\mathcal{C}_i, i \in \{1, 2\}$ of positively ($i = 1$) and negatively ($i = 2$) charged colloids, an approximation to the density profiles is

$$\varrho_i(\mathbf{r}) = \sum_{\mathbf{s}\in\mathcal{C}_i} \delta(\mathbf{r} - \mathbf{s}), \quad (6)$$

where δ is the Dirac delta. The energetic contribution to the Helmholtz free energy per particle, given by the term on the right-hand side of Eq. (5), follows directly from Eqs. (1) and (6); it is the analog for the screened Coulomb potential Eq. (1) of the well-known Madelung energy [15]. The hard-sphere Helmholtz free energy per particle, f^{hs}, is approximated by integrating the free-volume equation of state corresponding to crystal structure $\mathcal{C}$ of closed-packed packing fraction ϕ_{cp} [16] with respect to the packing fraction ϕ.

Finally the Helmholtz free energy per particle of crystal structure $\mathcal{C}$ reads

$$\begin{aligned} & f(T^*,\phi) \\ =\ & c_s + \ln(\phi) - 3\ln\left(1-\left(\frac{\phi}{\phi_{\mathrm{cp}}}\right)^{1/3}\right) \\ & + \frac{1}{2K_cT^*}\sum_{i,j} q_iq_j \sum_{(\mathbf{s},\mathbf{s}')\in\mathcal{C}^*_{ij}} \frac{\exp(-\kappa a(|\mathbf{s}-\mathbf{s}'|/a-2))}{|\mathbf{s}-\mathbf{s}'|/a} \end{aligned} \tag{7}$$

with the number of colloids per unit cell K_c and the abbreviation $\mathcal{C}^*_{ij} = \{(\mathbf{s},\mathbf{s}') \in \mathcal{C}_i \times \mathcal{C}_j : \mathbf{s}' \in W_{\mathcal{C}}, \mathbf{s} \neq \mathbf{s}'\}$, where $W_{\mathcal{C}}$ denotes the unit cell. The integration constant c_s in Eq. (7) is *independent* of the closed-packed packing fraction ϕ_{cp} and the crystal structure $\mathcal{C}$.

3. *Substitutionally disordered solid phase*

The density profiles of a crystal structure $\mathcal{C}$ with the sites occupied randomly by positively and negatively charged colloids with probability x_1 and x_2, respectively, are approximated, in place of Eq. (6), by

$$\varrho_i(\mathbf{r}) = x_i \sum_{\mathbf{s}\in\mathcal{C}} \delta(\mathbf{r}-\mathbf{s}). \tag{8}$$

Therefore, the Helmholtz free energy per particle is approximated by

$$\begin{aligned} & f(T^*,\phi,x) \\ =\ & c_s + \sum_i x_i\ln(x_i) + \ln(\phi) - 3\ln\left(1-\left(\frac{\phi}{\phi_{\mathrm{cp}}}\right)^{1/3}\right) \\ & + \frac{(2x-1)^2}{2K_cT^*} \sum_{(\mathbf{s},\mathbf{s}')\in\mathcal{C}^*} \frac{\exp(-\kappa a(|\mathbf{s}-\mathbf{s}'|/a-2))}{|\mathbf{s}-\mathbf{s}'|/a} \end{aligned} \tag{9}$$

with $\mathcal{C}^* = \{(\mathbf{s},\mathbf{s}') \in \mathcal{C} \times \mathcal{C} : \mathbf{s}' \in W_{\mathcal{C}}, \mathbf{s} \neq \mathbf{s}'\}$. Note the "entropy of mixing" contribution due to the random occupation of sites and that the screened-Coulomb energy vanishes at $x = 1/2$ for the present choice of equally sized, oppositely charged particles.

4. *Hard-sphere freezing*

In order to fix the values of the integration constants c_f (see Eq. (4)) and c_s (see Eqs. (7) and (9)) it is required that hard-sphere freezing from a fluid to a random face-centered cubic (rfcc) phase, i.e., a substitutionally disordered solid, takes place in the limit $T^* \to \infty$ at $p^*_{\mathrm{coex}} = 11.54(4)\pi/6 \approx 6.042$ (see Ref. [17]). As the Gibbs free energies per particle of the fluid and the rfcc solid must be equal at coexistence, the two constants c_f and c_s are related by $c_f - c_s \approx 1.084$. As only differences of Gibbs free energies are relevant in order to determine the equilibrium state, we set $c_s = 0$ without restriction of generality. The binodals of the fluid-rfcc solid coexistence region at high temperatures are found to be located at packing fractions $\phi_{\mathrm{f}} \approx 0.4916, \phi_{\mathrm{rfcc}} \approx 0.5547$, i.e., the coexistence region is in good agreement with that found in computer simulations [17], albeit slightly wider.

structure	c/d	K_c	ϕ_{cp}
$\mathrm{CaF_2}$	c	3	$3\pi\sqrt{3}/32$
CsCl	c	2	$\pi\sqrt{3}/8$
CuAu	c	2	$\pi(2+(c/a)^2)\sqrt{1+2(a/c)^2}/24$
$\mathrm{Cu_3Au}$	c	4	$\pi\sqrt{2}/6$
$\mathrm{LS_6^{fcc}}$	c	7	$7\pi\sqrt{2}/48$
NaCl	c	2	$\pi/6$
NbP	c	8	$\pi\sqrt{2}/6$
rbcc	d	1	$\pi\sqrt{3}/8$
rfcc	d	1	$\pi\sqrt{2}/6$

TABLE I: Candidate solid structures chosen on the basis of Refs. [7, 9–12]. For detailed structure information see Ref. [18]. The second column indicates a crystal ("c") or a substitutionally disordered solid ("d"). The third and the fourth columns give the numbers of particles per unit cell K_c and the closed-packed packing fractions ϕ_{cp}, respectively. The CuAu structure with the aspect ratio $c/a \in [1, \sqrt{2}]$ of the underlying tetragonal lattice degenerates to the CsCl structure in the case $c/a = 1$. The $\mathrm{LS_6^{fcc}}$ structure has been introduced in Ref. [19]. The NbP structure was called "tetragonal" in Ref. [10].

C. Phase diagrams

In order to calculate phase diagrams in terms of T^*, p^*, and x a set of candidate solid structures is chosen in the next section. Let $\tilde{g}(T^*, p^*, x)$ be defined as the minimum of the Gibbs free energies per particle constructed in the previous subsection of the fluid, the candidate crystals, and the candidate substitutionally disordered solids for given (T^*, p^*, x). The equilibrium Gibbs free energy is the convex hull of $\tilde{g}(T^*, p^*, x)$ as a function of $x \in [0, 1]$, which can be readily constructed numerically on a x-grid. During this calculation the coexistence regions of the phase diagrams can be identified as the set of state points where Maxwell's common tangent construction applies.

The Gibbs free energies per particle as defined in the previous subsection exhibit an unphysical feature at low pressures, where for all temperatures the fluid becomes apparently unstable with respect to an rfcc crystal; the reason for this phenomenon is related to the well-known incorrect low-density asymptotics of the free-volume equation of state [16]. In order to resolve this problem it is assumed that once a stable fluid state for given (T^*, p^*, x) is found, a stable fluid state is also assumed for (T^*, x) and all pressures smaller than p^*.

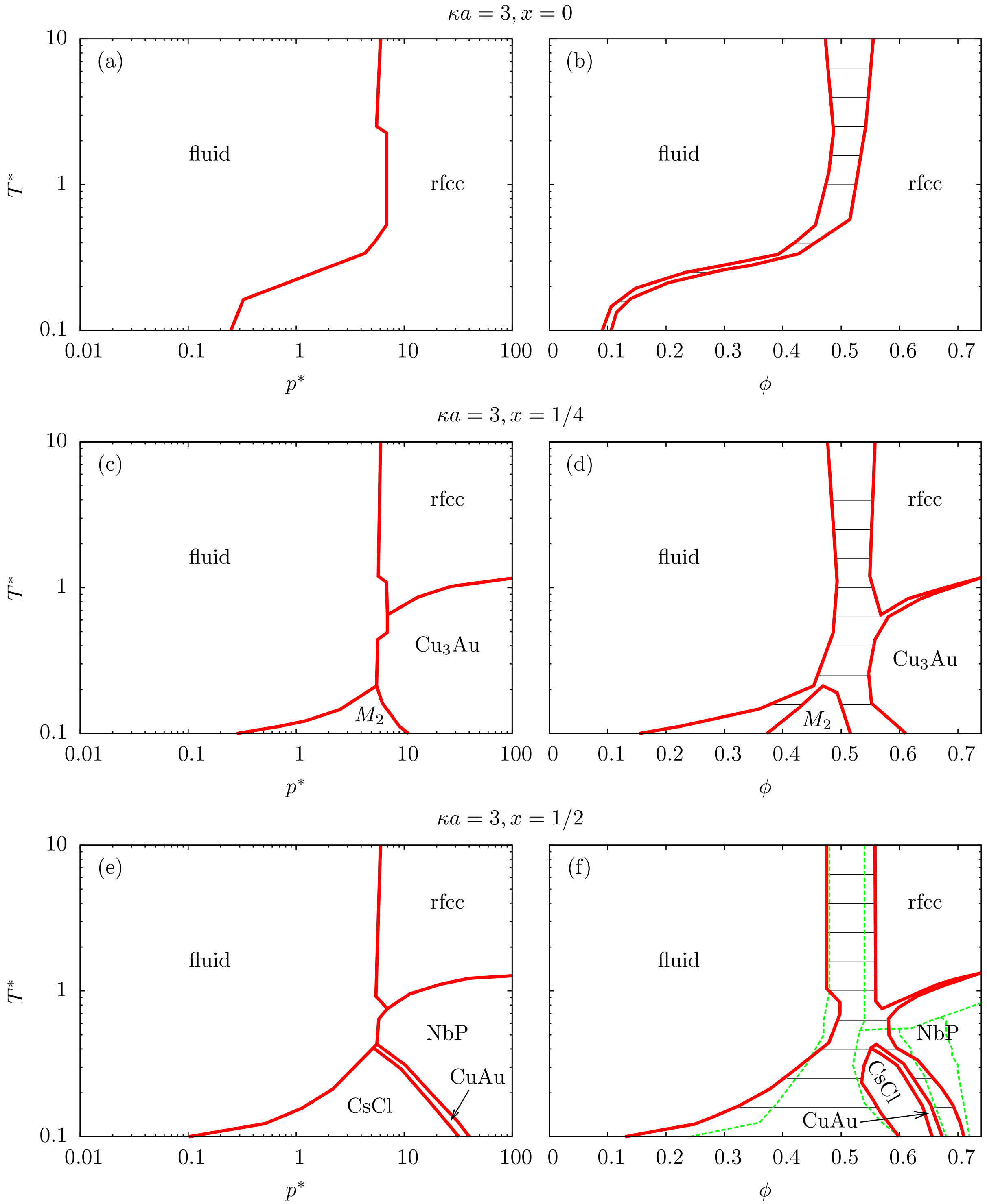

FIG. 1: Phase diagrams for $\kappa a = 3$ at compositions x in terms of (T^*, p^*) and (T^*, ϕ). The green dashed lines in panel (f) reproduce the phase diagram of the computer simulation study of Ref. [10]. Labels of pure solid phases correspond to Tab. I. Panels (c) and (d) exhibit a two-phase coexistence region $M_2 = \mathrm{CsCl} + \mathrm{rfcc}$. Horizontal thin lines in panels (b), (d), and (f) are tie lines.

III. RESULTS AND DISCUSSION

Table I lists the candidate solid structures considered here. This choice is based on the structures found in computer simulation studies of the cases $x = 0$ (see Ref. [9]) and $\kappa a = 3, x = 1/2$ (see Ref. [10]), as well as on Refs. [7, 11, 12], where the limit $T^* \to 0$ is ad-

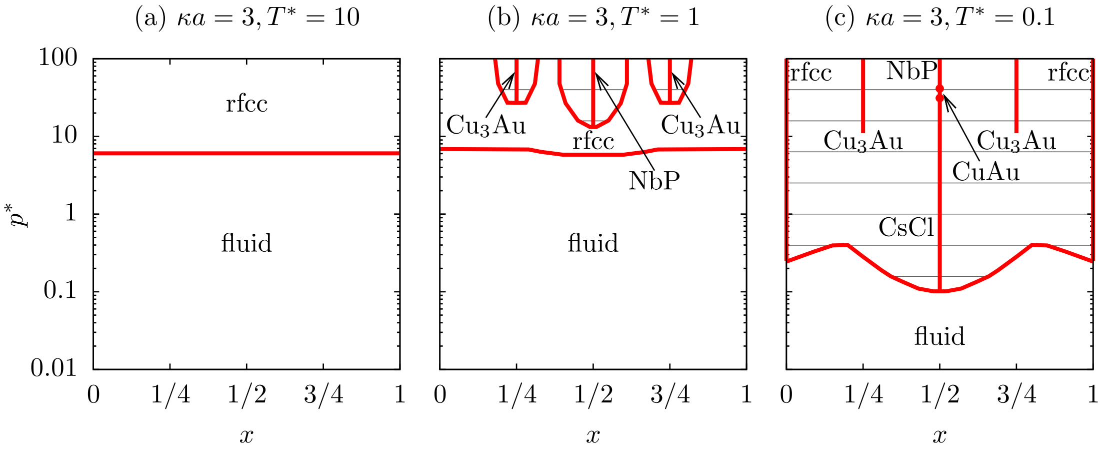

FIG. 2: Phase diagrams for $\kappa a = 3$ in terms of (p^*, x) at temperatures (a) $T^* = 10$, (b) $T^* = 1$, and (c) $T^* = 0.1$ (see also Fig. 1). Horizontal thin lines in panels (b) and (c) are tie lines.

dressed by means of Madelung energy sums. Moreover, the CsCl (cesium chloride), CuAu (copper gold), NaCl (sodium chloride), and Cu$_3$Au structures have been identified in experiments [7, 8]. Table I indicates whether the solid is crystalline ("c") or substitutionally disordered ("d") and it exhibits the numbers of particles per unit cell K_c as well as the closed-packed packing fractions ϕ_{cp}. Detailed structure information can be found in Ref. [18]. The CuAu structure, which is described by a tetragonal lattice of aspect ratio $c/a \in [1, \sqrt{2}]$ and a two-particle basis, degenerates to the CsCl structure in the case $c/a = 1$. The structure denoted by LS_6^{fcc} was introduced in Ref. [19] and the NbP (niobium phosphide) structure was called "tetragonal" in Ref. [10].

A. Case $\kappa a = 3$

The phase diagrams for the case $\kappa a = 3$ in terms of (T^*, p^*) and (T^*, ϕ) at compositions $x = 0$, $x = 1/4$, and $x = 1/2$ are displayed in Fig. 1. Thick solid lines represent phase boundaries whereas thin horizontal lines in (T^*, ϕ) diagrams (panels (b), (d), and (f)) are tie lines connecting coexisting states. At low temperatures two-phase coexistence $M_2 := \text{CsCl} + \text{rfcc}$ is found (see Figs. 1(c) and (d)).

By construction a fluid-rfcc transition takes place for any κa and x in the limit $T^* \to \infty$ at the coexistence pressure p^*_{coex} and volume fractions ϕ_{f} and ϕ_{rfcc} (see Sec. II B 4). For $T^* \to 0$ and $x = 1/2$ a CsCl crystal coexists with a dilute gas, in agreement with Ref. [12] because the free energy of the present formalism reduces to Madelung-like energy sums in this limit. A cut of the phase diagrams at composition $x = 0$ is shown in Figs. 1(a) and (b), which involves merely the fluid and the rfcc structures, which is consistent with computer simulation results [9]. Figures 1(c) and (d) display a cut at $x = 1/4$, with an additional Cu$_3$Au phase as well as the two-phase coexistence region M_2. The structures at composition $x = 1/4$ differ from those at composition $x = 3/4$ only by an exchange of the colloid species ($1 \leftrightarrow 2$).

In order to assess the reliability of the approach described in Sec. II, Fig. 1(f) compares the calculated phase diagram (red solid lines) in terms of (T^*, ϕ) for $\kappa a = 3, x = 1/2$ with that obtained by means of free energy calculations using computer simulations in Ref. [10] (green dashed lines). Both studies agree in the predicted stable structures fluid, rfcc, CsCl, CuAu, and NbP. The overall topology is similar for both approaches; however, the present formalism overestimates the stability of the NbP structure leading to a fluid-NbP transition (see Figs. 1(e) and (f)) which is not observed in the computer simulation. Moreover, our formalism leads to a fluid-CuAu transition in a very narrow window around $T^* \approx 0.4$ but no rfcc-CuAu transition is found, whereas it is the opposite situation with the computer simulation results. Agreement between mean-field theory and computer simulation is observed with respect to the order of the phase transitions: The CsCl-CuAu transition is of second order because the CuAu structure transforms continuously into CsCl upon $c/a \to 1$, and the other phase transitions are of first order. Both the rfcc-NbP and the CuAu-NbP phase transitions are described as "weakly first-order" in Ref. [10], whereas within our approach, only the rfcc-NbP transition exhibits a very narrow but non-vanishing ϕ-gap and the CuAu-NbP transitions is strongly first-order (see Fig. 1(f)). The quantitative disagreement in the strength of the first-order CuAu-NbP transition can be understood on the basis of a smearing out of structural differences due to fluctuations, which are present in computer simulations but which are not fully accounted for by mean-field theories. This comparison between the formalism of Sec. II and the computer simulation study of Ref. [10] for the special case $\kappa a = 3, x = 1/2$ shows that, apart from well-known defects of mean-field theories, the present approach is semi-quantitatively reliable. Moreover, the simplicity of the

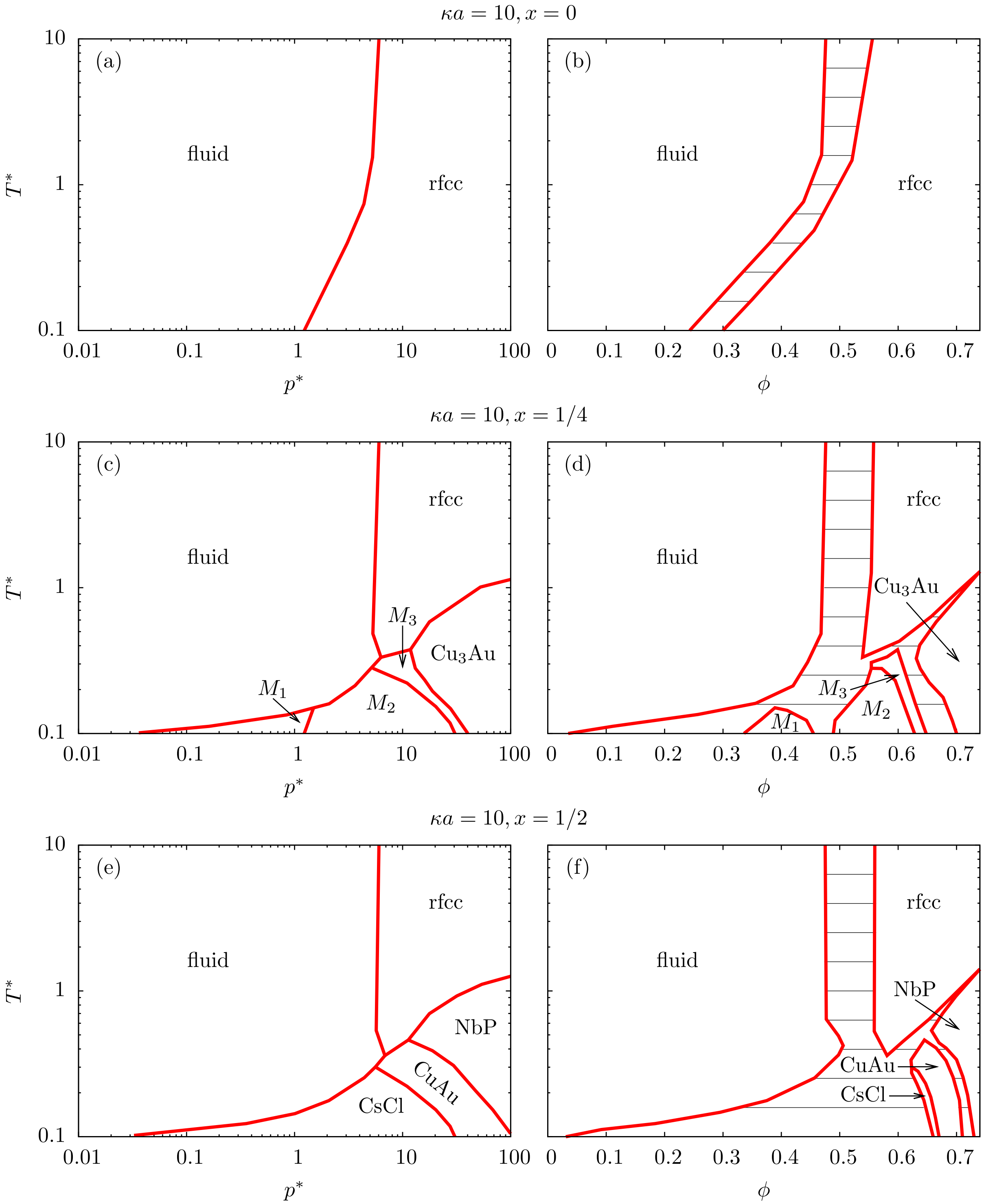

FIG. 3: Phase diagrams for $\kappa a = 10$ at compositions x in terms of (T^*, p^*) and (T^*, ϕ). Labels of pure solid phases correspond to Tab. I. Panels (c) and (d) exhibit two-phase coexistence regions M_1 = CsCl+fluid, M_2 = CsCl+rfcc, and M_3 = CuAu+rfcc. Horizontal thin lines in panels (b), (d), and (f) are tie lines.

present formalism gives computational advantages over computer simulations such that now complete phase diagrams in terms of (T^*, p^*, x) as a function of the parameter κa can be determined readily.

Figure 2 displays the phase diagram for $\kappa a = 3$ in terms of (p^*, x) for temperatures (a) $T^* = 10$, (b) $T^* = 1$, and (c) $T^* = 0.1$. At high temperatures (see Fig. 2(a)) only fluid and rfcc structures are present and the fluid-rfcc transition line becomes independent of the composition x in the limit $T^* \to \infty$. At lower temperatures (see Figs. 2(b) and (c)) CsCl, CuAu, Cu_3Au, and NbP crystal structures occur at fixed compositions. At low temperatures and pressures as well as strongly asymmetric mixtures (see Fig. 2(c) for $p^* < 1$ and $x < 1/4$ or $x > 3/4$) the MSA approximation applied to model the fluid phase leads to an unphysical artifact which exhibits the apparent coexistence of an almost pure rfcc crystal with a less pure fluid. The reason for this unphysical phenomenon is that under these conditions the MSA pair distribution function becomes negative such that an increasing repulsive interaction potential leads to a more and more negative, i.e., attractive, contribution to the free energy. However, outside of this range of the phase diagram MSA leads to a physically reasonable description of the fluid phase. The full phase diagram for $\kappa a = 3$ in terms of (T^*, p^*, x) can be inferred from the two-dimensional cuts in Figs. 1 and 2.

B. Case $\kappa a = 10$

In order to study the changes of the phase diagram upon changing the screening strength κa, the phase diagrams for various screening strengths $\kappa a \in \{2, 3, 5, 10\}$ have been calculated. The trends in the variations of the phase diagrams upon changing κa are found to be monotonic such that it is sufficient in the following to consider the case $\kappa a = 10$.

Figures 3 displays the phase diagram for $\kappa a = 10$ in terms of (T^*, p^*) and (T^*, ϕ) at compositions $x = 0$, $x = 1/4$, and $x = 1/2$. Two-phase coexistence regions $M_1 :=$ CsCl + fluid, $M_2 =$ CsCl + rfcc, and $M_3 :=$ CuAu + rfcc are present in Figs. 3(c) and (d). By comparison of Figs. 1 and 3 one infers a shift of the rfcc phase to lower temperatures upon increasing κa. This observation can be understood by the fact that the interaction potential is approaching the hard-sphere potential in the limit $\kappa a \to \infty$. The Cu_3Au phase in Figs. 1(c) and 3(c) or Figs. 1(d) and 3(d) shrinks upon increasing κa, which is partly due to the growing rfcc phase. Figures 1(e) and 3(e) or Figs. 1(f) and 3(f) exhibit an increasing temperature range of stability of the CuAu structure upon increasing κa. As a consequence the NbP phase, located in between the extending rfcc and CuAu phases, shrinks upon increasing κa. Moreover, upon increasing κa, the fluid-NbP transition disappears and an rfcc-CuAu coexistence is established. Finally, the ϕ range of the CsCl phase becomes smaller upon increasing κa as can be inferred from Figs. 1(f) and 3(f).

In order to make predictions on the conditions to synthesize certain crystal structures, it is expected within the present formalism that colloids with strongly screened Coulomb interaction, i.e., large values of κa, are preferable to prepare CuAu structures, whereas CsCl, Cu_3Au, and NbP crystals are expected to be found most easily in systems of weakly screened Coulomb interaction. Given a certain crystal structure has been prepared, the above reasoning leads to the following conclusions: CuAu structures become more whereas CsCl, Cu_3Au, and NbP structures become less stable against temperature variations upon increasing κa.

IV. SUMMARY

In this work a simple, yet semi-quantitative mean-field theory for binary colloidal mixtures of spherical particles of equal radii and opposite charges has been described and applied to calculate the global phase diagrams in terms of temperature, pressure and composition for various screening strengths (see Figs. 1–3). The formalism interpolates between the hard-sphere limit at high temperatures and a Madelung-like description at low temperatures. The reliability of the method has been checked by comparison with computer simulation results [9, 10] for one single composition and screening strength as well as with Madelung sum calculations [7, 11, 12] in the low-temperature limit. Limitations of the present formalism can be understood as a result of the absence of fluctuations within mean-field theories and properties of the mean-spherical approximation (MSA). The influence of the screening strength on the stability of crystalline phases has been discussed, which has implications, e.g., on the preparation procedure and the choice of experimental conditions.

An extension of the presented theory to multicomponent, size- and charge-polydisperse colloidal suspensions along the lines described in Sec. II is straightforward as the free volume equation of state used for the solid phases does not explicitly depend on the colloid radii and more general formulations of the MSA are available [20, 21]. It is therefore a matter of choosing an appropriate set of candidate solid structures (see Tab. I), which could be motivated by findings from experiments and computer simulations of special cases.

Acknowledgments

MB thanks A. Maciołek for helpful comments. MD acknowledges financial support from an NWO-vici grant. This work is part of the research program of the "Stichting voor Fundamenteel Onderzoek der Materie (FOM)", which is financially supported by the "Nederlandse Organisatie voor Wetenschappelijk Onderzoek (NWO)".

---

[1] P. Habdas and E. R. Weeks, Curr. Opin. Colloid Interface Sci. **7**, 196 (2002).

[2] B. V. R. Tata and S. S. Jena, Solid State Commun. **139**,

562 (2006).

[3] V. Prasad, D. Semwogerere, and E. R. Weeks, J. Phys.: Condens. Matter **19**, 113102 (2007).

[4] Y. Liang, N. Hilal, P. Langston, and V. Starov, Adv. Colloid Interface Sci. **134-135**, 151 (2007).

[5] M. Dijkstra, Curr. Opin. Colloid Interface Sci. **6**, 372 (2001).

[6] A. Yethiraj and A. van Blaaderen, Nature **421**, 513 (2003).

[7] M. E. Leunissen, C. G. Christova, A.-P. Hynninen, C. P. Royall, A. I. Campbell, A. Imhof, M. Dijkstra, R. van Roij, and A. van Blaaderen, Nature **437**, 235 (2005).

[8] E. V. Shevchenko, D. V. Talapin, N. A. Kotov, S. O'Brien, and C. B. Murray, Nature **439**, 55 (2006).

[9] A.-P. Hynninen and M. Dijkstra, Phys. Rev. E **68**, 021407 (2003).

[10] A.-P. Hynninen, M. E. Leunissen, A. van Blaaderen, and M. Dijkstra, Phys. Rev. Lett. **96**, 018303 (2006).

[11] G. R. Maskaly, R. E. García, W. C. Carter, and Y.-M. Chiang, Phys. Rev. E **73**, 011402 (2006).

[12] D. van den Berg, Master thesis, Utrecht University, 2009.

[13] M. Ginoza, Mol. Phys. **71**, 145 (1990).

[14] N. F. Carnahan and K. E. Starling, J. Chem. Phys. **51**, 635 (1969).

[15] C. Kittel, *Introduction to Solid State Physics* (Wiley, New York, 1996).

[16] W. W. Wood, J. Chem. Phys. **20**, 1334 (1952).

[17] E. G. Noya, C. Vega, and E. de Miguel, J. Chem. Phys. **128**, 154507 (2008).

[18] `http://cst-www.nrl.navy.mil/lattice`

[19] A.-P. Hynninen, C. G. Christova, R. van Roij, A. van Blaaderen, and M. Dijkstra, Phys. Rev. Lett. **96**, 138308 (2006).

[20] L. Blum, F. Vericat, and J. N. Herrera-Pacheco, J. Stat. Phys. **66**, 249 (1992).

[21] M. Ginoza and M. Yasutomi, J. Stat. Phys. **90**, 1475 (1998).